PROCEEDINGS OF SPIE

SPIEDigitalLibrary.org/conference-proceedings-of-spie

Measurement and modelling of the chromatic dependence of a reflected wavefront on the Euclid space telescope dichroic mirror

M. Baron, B. Sassolas, P.-A. Frugier, L. Gaspar Venancio, J. Amiaux, et al.

M. Baron, B. Sassolas, P.-A. Frugier, L. M. Gaspar Venancio, J. Amiaux, M. Castelnau, F. Keller, G. Dovillaire, P. Treimany, R. Juvénal, L. Miller, L. Pinard, A. Ealet, "Measurement and modelling of the chromatic dependence of a reflected wavefront on the Euclid space telescope dichroic mirror," Proc. SPIE 12180, Space Telescopes and Instrumentation 2022: Optical, Infrared, and Millimeter Wave, 121804V (27 August 2022); doi: 10.1117/12.2630072

SPIE.

Event: SPIE Astronomical Telescopes + Instrumentation, 2022, Montréal, Québec, Canada

Downloaded From: https://www.spiedigitallibrary.org/conference-proceedings-of-spie on 06 May 2023 Terms of Use: https://www.spiedigitallibrary.org/terms-of-use

Measurement and modelling of the chromatic dependence of a reflected wavefront on the *Euclid* space telescope dichroic mirror

M. Baron[*a], B. Sassolas[a], P.-A. Frugier[b], L. M. Gaspar Venancio[c], J. Amiaux[d], M. Castelnau[e], F. Keller[c], G. Dovillaire[f], P. Treimany[f], R. Juvénal[f], L. Miller[g], L. Pinard[a], A. Ealet[a], on behalf of the Euclid Consortium

[a]Univ Lyon, Univ Claude Bernard Lyon 1, CNRS/IN2P3, IP2I Lyon - LMA, UMR 5822, F-69622, Villeurbanne, France
[b]AIM, CEA, CNRS, Université Paris-Saclay, Université Paris Diderot, Sorbonne Paris Cité, F-91191 Gif-sur-Yvette, France
[c]European Space Agency / ESTEC, Keplerlaan 1, 2201 AZ Noordwijk, The Netherlands
[d]IRFU, Service d'Astrophysique, CEA Saclay, F-91191 Gif-sur-Yvette Cedex, France
[e]Centre National d'Etudes Spatiales, 18 avenue Edouard Belin, F-31401 Toulouse Cedex 9, France
[f]Imagine Optic (IO), 91400 Orsay, France
[g]Dept. of Physics, Univ. Oxford, Keble Road, Oxford, OX1 3RH, UK

ABSTRACT

Euclid is the second M-class mission of ESA's Cosmic Vision Program. It implements a space telescope to be launched at L2. The objective is to characterize the dynamics of the early Universe by using two instruments: the high definition camera VIS (visible instrument) and the spectrophotometer NISP (Near Infrared Spectrometer and Photometer). Light entering *Euclid* is either reflected toward VIS in the visible band, or transmitted to NISP in the infrared band by a dichroic mirror. In order to guarantee the quality of scientific data delivered by the mission, the knowledge of any chromatic dependence of the optical payload's Point-Spread function (PSF) is critical. However, previous works showed that complex coatings, such as high-performance dichroic coating, are likely to induce high chromatic variations in reflection, either as a chromatic "Wave-Front-error" (WFE) and/or as inhomogeneous reflectance profile (*R*), both affecting PSF morphology. In-depth knowledge of the reflected wavefront by the *Euclid* Dichroic is then necessary in order to calibrate the in-flight *Euclid* Observations. This work focuses on two aspects. On the one hand, we present an experimental campaign to measure the dichroic WFE and *R* at any wavelength, incidence, and polarization state, with an extreme precision. This metrology work implements a bench funded by ESA, designed by Imagine Optic Company, and commissioned at LMA. On the other hand we build a numerical model of the dichroic based on these on-ground measurements. By reproducing the experimental optical properties of the dichroic mirror, we ensure the subjacent thin-films physics at play is well understood, ultimately providing adequate inputs for the in-flight calibration of *Euclid* with a suitable level of accuracy.

Keywords: *Euclid* telescope, dichroic coating, multilayer coatings, optical metrology, WaveFront Error, chromatic Point-Spread Function, Thickness non-uniformity.

1. INTRODUCTION

1.1 *Euclid* space telescope and its scientific mission

The *Euclid* payload module implements two cosmological probes: weak-lensing and galaxy clustering. Weak-lensing[1,2,3,4] consists in a statistic analysis of apparent average ellipticity of galaxies. Deviation to the expected morphology statistics can be interpreted as the presence of an over (or under) density of dark matter, which acts gravitationally on propagating light rays, distorting galaxy images. Galaxy clustering[1,5] is the analysis of the 3D galaxy distribution, where galaxy distances are derived from their spectroscopic redshifts. This probe aims at unraveling the dynamics of the Universe, which depends on its initial conditions, its curvature, and the quantity of dark energy and dark

Space Telescopes and Instrumentation 2022: Optical, Infrared, and Millimeter Wave, edited by Laura E. Coyle, Shuji Matsuura, Marshall D. Perrin, Proc. of SPIE Vol. 12180, 121804V · © 2022 SPIE · 0277-786X · doi: 10.1117/12.2630072

Downloaded From: https://www.spiedigitallibrary.org/conference-proceedings-of-spie on 06 May 2023
Terms of Use: https://www.spiedigitallibrary.org/terms-of-use

matter present at any time. The Euclid Consortium implements and combines these two probes, with an extreme precision, and this thanks to two *Euclid* instruments working together: VIS (Visible Instrument), and NISP (Near Infrared Spectrometer and Photometer). A dichroic mirror placed upstream of both instruments reflects the visible band towards VIS. In what follows, we will focus on the VIS performance only.

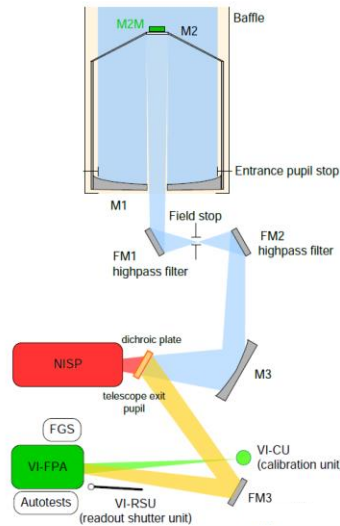

Figure 1: Schematic[6] of the *Euclid*'s Payload Module (PLM) sub-systems, Courtesy Airbus Defence and Space. https://www.euclid-ec.org/?page_id=2639

1.2 Point-Spread Function

The knowledge of Euclid PSF is a key to the weak-lensing probe, since it causes systematic effects on the measurement of the morphology of the galaxies. In order to correct for these fundamental source of systematics, the *Euclid* Science Ground Segment (SGS) pipelines require an excellent knowledge of the PSF itself.

By design, the *Euclid* dichroic is located at VIS pupil plane. In this case, the PSF can be inferred[4,7] from a pupil function which is directly affected by the dichroic-induced WFE(x, y, λ) and $R(x, y, \lambda)$ in reflection. This means that WFE and R high chromatic dependences[8], induced by the non-uniformities on the coating stack, lead to additional PSF complexity known to be sufficiently significant to justify a dedicated metrology work.

Let's consider a coating where the thickness of the layers slightly differs at any location on the surface of each layer, characterized by a Thickness Figure Error (TFE). The phase shift φ_R becomes then spatially dependent. In this case, the reflected wavefront is not perfectly flat anymore, as should be the incident wavefront. It presents then a non-zero WFE[7,9] in reflection. It is very important to know the induced WFE contribution of the dichroic mirror at each lambda. The reflectance chromaticity $R(x, y, \lambda)$ can also affect the PSF spectral behavior by apodization of the reflectance in the exit pupil. More specifically, this dependence is critical near the edges of the optical bandpass filter, where the reflectivity goes from 0% to almost 100% in a few nanometers.

1.3 Dichroic chromaticity numerical model

In addition to the WFE metrology with the dedicated bench, a model will be developed for the prediction of the chromatic effects induced by the dichroic. This model, calibrated with bench measurements (in controlled configurations: single-wavelength, incidence… and controlled environment: temperature, vibration…) shall allow the prediction of the spectral behavior of the component from its TFEs, under any illumination configuration, in particular the in-flight illumination configurations. Its purpose is to predict the WFE, R, the two ingredients for the PSF calculation, with their respective chromatic dependence. This model will be also tunable with adjustable parameters to make the further transition between the flight model and the (measured) spare component, which inevitably have physical differences. The specific illumination conditions of the component in flight do not allow direct measurements of WFE, R, and PSF at a single wavelength, making it even more useful to implement a model that can trace back to these physical quantities. Finally, the last advantage of the model is to access the geometry of the stack thin layers non-uniformities, the fundamental physical cause of the chromatic behavior, information that is not directly accessible by raw WFE or R measurements.

Downloaded From: https://www.spiedigitallibrary.org/conference-proceedings-of-spie on 06 May 2023
Terms of Use: https://www.spiedigitallibrary.org/terms-of-use

1.4 *Euclid* beamsplitter and thin-films technology

From the VIS perspective, the dichroic is a "bandpass" mirror with a useful diameter of 113 mm, and whose peculiarity is that it is reflective for visible light ([550, 900] nm wavelength range) towards VIS, and on the contrary transmittive for infrared light ([920, 2000] nm wavelength range). Thin-film theory is well described[7,10,11,12] and can be used to compute any spectral properties of a thin-film stack. For any illumination condition (wavelength λ, incidence angle γ, and polarization state $Pol.$) it is possible to compute the reflectivity "R" as the amount of reflection in intensity.

$$R(x, y, \lambda, \gamma, Pol.) \coloneqq |r(x, y, \lambda, \gamma, Pol.)|^2 , \tag{1}$$

with $r(x, y, \lambda, \gamma, Pol)$ being the complex reflection coefficient of the electric field, related to the coating properties (thicknesses, refractive indices). Additionally, a phase shift occurs between the reflected and incident electric field. In the case of a metallic mirror, this phase shift is π radians, independently of λ, γ, P. Quite the opposite, the spectral phase shift[11] is much more complex for a dielectric coating depending both on stack properties, illumination conditions, and expressed by:

$$\varphi_{\mathrm{R}}(\lambda, \dots) \coloneqq \arg[r(\lambda, \dots)] . \tag{2}$$

We will see further in this article why this phase shift is a crucial quantity for the optical performance.

1.5 Manufacturing process for *Euclid* dichroic

The dichroic coating deposited onto the front surface of the dichroic plate was produced[13,14] with an extreme precision by Optical Balzers Jena (OBJ) Company and meets the stringent ESA requirements[13]. The 10 µm thick coating is composed by almost 200 layers of Nb_2O_5 and SiO_2 deposited on a fused silica substrate. On the back side, an antireflective coating was deposited with the same materials and approximatively the same number of layers. To create the coatings, OBJ used the PARMS process[14] (Plasma Assisted Reactive Magnetron Sputtering), in a vacuumed "Helios machine"[14], driven by a deposition control "OMS 5000"[14] (Optical Monitoring System). Fig. 2 shows schematically how this process works.

Although the process used by OBJ is extremely accurate, there are still some small imperfections in the deposition for each layer. Indeed, the two sputters cannot apply a perfectly homogeneous layer at each point on the substrate. There remains in any case some spatial inhomogeneity in the plume of each sputter. This has an impact of the whole coating, leading to spatial thickness non-uniformity for each layer, i.e. a "TFE". The TFE peak-to-valley (PTV) should not exceed 0.5% in thickness[9]. As the total stack is 10 µm thick, the absolute PTV is around 50 nm.

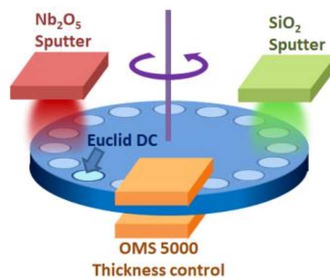

Figure 2: Schematic representation of PARMS process applied to *Euclid* dichroic with OBJ's Helios machine.

2. MEASUREMENT OF THE *EUCLID* DICHROIC OPTICAL PROPERTIES

2.1 High precision metrology

The WFE measurement of *Euclid* dichroic is very challenging, due to the extreme ESA and CNES specifications and the wide panel of measurements needed. The main functions of the bench are: reflected WFE measurement, Intensity mapping and PSF mapping. All these measurements shall be achieved for all illumination configurations. An illumination configuration means one wavelength at one angle of incidence and in one linear polarization state. The bench operates under very specific and controlled conditions, which allow the precise characterization of the dichroic WFE and calibration of the numerical model. Additional calibration will be necessary to be placed in "flight" configuration.

Downloaded From: https://www.spiedigitallibrary.org/conference-proceedings-of-spie on 06 May 2023
Terms of Use: https://www.spiedigitallibrary.org/terms-of-use

For any configurations, the WFE shall be measured on the whole diameter with a metrological precision of 2 nm RMS. The WFE induced by the metrology bench itself has to be known better than 1.5 nm RMS. In other words, the resulting needed precision is about $\lambda/400$. In addition, the bench shall spatially describe the WFE using the 55 first Noll-Zernikes, and this by using a "Shack-Hartmann" sensor (SH).

Furthermore, Reflectance maps shall be obtained for each configuration, with a high-definition camera (1024*1024 pixels). The collimated beam intensity profile shall be known at 0.1% on each point of the camera, before and after reflection on the component.

Last, the PSF of the test bench, including dichroic component, will be imaged by a dedicated channel. This will ensure adequate ingestion of WFE/R data into PSF models. Also, slight defocuses can be added on this channel to infer WFE and PSF through phase-diversity algorithms[15]. The work presented in this paper focuses only on WFE and *R* measurements.

Section	Parameter	Interval	Precision
Illumination configurations	Wavelength	510 to 950 nm	Central wavelength : 0.1 nm Spectral width : 0.4 nm FWMH
	Polarization	S and P	0.5 deg.
	Incidence	0 deg.; 4 to 20 deg.	0.005 deg.
WaveFront Error channel	Dichroic WFE	All illumination configurations	2 nm RMS
	Bench WFE	All illumination configurations	1.5 nm RMS
Intensity channel	Reflectance map	All illumination configurations	1024*1024 pixels Intensity profile known at 0.1%
PSF channel	PSF map	All illumination configurations	1024*1024 pix. SNR of 500

Table 1: Main technical specifications imposed on *Euclid* dichroic flight spare test bench. A "spectral configuration" means one wavelength at one specific incidence with one linear polarization.

Many aspects have to be controlled in order to reach the challenging very low uncertainties, and chief among them environmental constraints. Indeed it has been determined by ESA that an ISO-3 clean room[16] is needed to guarantee compliant micro-particle density and environmental stability. That is why the metrology setup will be installed in the LMA[17] (Laboratoire des Matériaux Avancés) ISO-3 clean room.

2.2 Architecture of the metrology bench

The company Imagine Optic[18] (IO), specialized in optical technologies, has been chosen by ESA for the development and the manufacturing of OBSERVE (Optical Bench for Spectrally rEsolved Reflective Wavefront of *Euclid* dichroic) bench. The principle of OBSERVE is as follows:

- A white light source produces a continuous beam towards a high precision monochromator fiber. Then, the resulting monochromatic ray goes through a fiber up to the optical bench.
- After the fiber, the beam is then polarized and reshaped by an iris and a beam expander. The ray is thus collimated and sized in function of the dichroic diameter.
- The dichroic is placed on a rotation stage in order to tune the angle of incidence, and reflects the beam towards the "beam reducer" block. This beam reducer follows the same optical design as the beam expander. The resulting beam is collimated, with a diameter of few millimeters, adapted to the Shack-Hartmann (SH) sensor aperture.

Downloaded From: https://www.spiedigitallibrary.org/conference-proceedings-of-spie on 06 May 2023
Terms of Use: https://www.spiedigitallibrary.org/terms-of-use

- After a second polarizer for polarization analysis, the beam reaches either the WFE channel (Shack-Hartmann sensor) or the PSF channel. In this case, a convergent mirror is added before the Shack-Hartmann to focus the light beam. A CMOS camera is then placed in the focal plane to register the PSF figure.

For any configuration, it is possible to replace the dichroic with a flat metallic mirror as a reference flat. This mirror is used to have knowledge of some static errors: the WFE induced by the bench itself, and by the misalignment/decentering. The Surface Figure Error (SFE) of this mirror provided by Zeiss Company will be characterized precisely at LMA before its use. The reference will be known within 0.2 nm RMS thanks to wavelength-shifting interferometry at 1064 nm[19].

To be more accurate, two light sources will be used instead of one. One of the sources will be used as "reference" source. The strategy to estimate the WFE is to measure the difference between the WFE with the tunable polychromatic source and the WFE obtained with the (fixed) reference light source. This "tic-toc" strategy, proposed by IO, allows minimization of the air turbulence impact in the room.

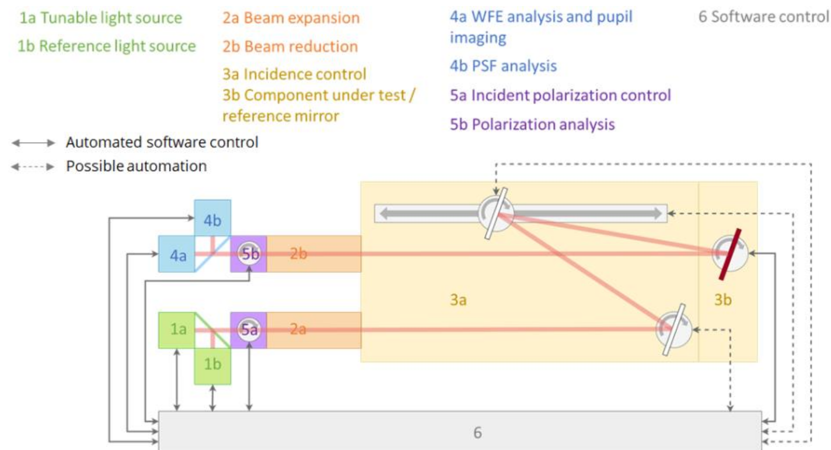

Figure 3: Schema of OBSERVE optical bench (top view) with legend. The "3b" red mirror in this image represents the localization of the dichroic or reference flat mirror, adjustable in rotation. The mirror on top of the schema can be rotated and translated on a rail, in order to maintain pupil conjugation for all incidences. Image credit: Imagine Optic.

The chosen "trombone" optical design, (represented on Fig. 3, block "3a") of the bench is an IO concept which main advantages are the compactness, the simplicity of movements (especially for incidence tuning), the one-block structure, and the ability to automate most of mechanical elements. Only 3 rotations and one translation (Fig. 3: "3a" block) are needed to tune the bench to one specific angle of incidence.

3. COATING NUMERICAL MODEL

3.1 Strategy of the model

As presented in the introduction, the model aims at predicting the dichroic chromatic dependence of the optical properties (WFE, R). The interests are multiple, firstly to facilitate the dichroic PSF knowledge in flight conditions, but also to add some knowledge of the stack non-uniformities (TFEs), the original source of PSF chromaticity. This last point is absolutely not restricted to the case of the dichroic itself. The strategy of the model is therefore apparently quite simple. We seek to numerically recreate the stack of thin films, with its whole TFEs, so that the resulting optical properties shall match with those measured with the bench. In the current state of this study, this fitting pipeline is applied to WFE only but may be extended to other properties such as R. and, so that, the fit will be even more constrained.

Downloaded From: https://www.spiedigitallibrary.org/conference-proceedings-of-spie on 06 May 2023
Terms of Use: https://www.spiedigitallibrary.org/terms-of-use

Obtaining a WFE from an optical coating is direct. With the nominal thicknesses and refractive indices of the thin-film stack plus the known TFE of each layer, we can build a model of a stack with non-uniformities. With the thin-films theory, it is possible to have the local phase shift, for any incidence, polarization, and wavelength at the level of each spatial position. Then, knowing all the phase shifts, the resulting WFE can be built, and compared to the measured WFE.

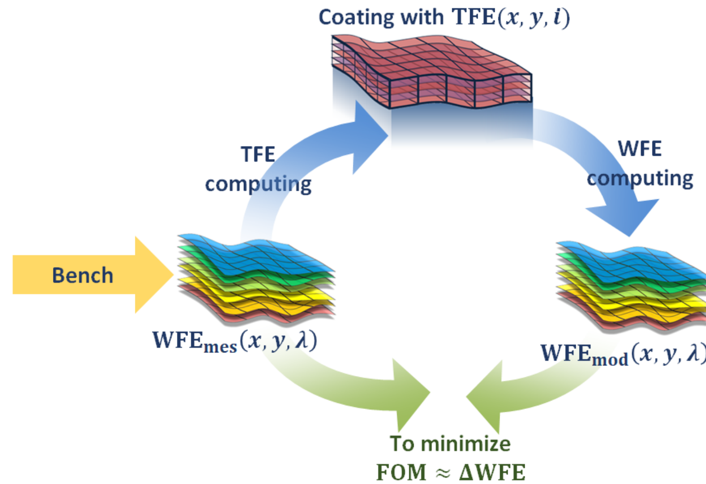

Figure 4: Shema of the strategy used to build the TFE/WFE model of the dichroic coating. The bench provides some "measured WFEs": WFE$_{mes}(x, y, \lambda)$ and the model fits a "modelled WFE": WFE$_{mod}(x, y, \lambda)$

Then, challenge is to make the modelled WFE correspond to the measured one. Indeed, the mathematical approach used to calculate the phase shifts and reflectance from the coating properties is not uniquely reversible. The optical parameters result from a matrix product of 200 terms (one matrix per layer), but there is no way to re-obtain all the matrices from optical parameters directly.

A brute-force method for fitting the WFE without any hypothesis or assumption is very difficult. For example, if each of almost 200 layer has a TFE modelled with 50 parameters (like Zernike polynomials), this leads to almost 10 000 inputs to setup the model. Such method would be time-consuming and could exhibit convergence problems. This is why we propose to reduce the number of degrees of freedom of the model.

3.2 Homothetic assumption

The simplest hypothesis is the **homothetic assumption**[20]. In this case, we suppose the TFE of all layers are the same, regardless of the material, and only weighted by the layer thickness. Knowing all the thicknesses, the number of unknown values to define the whole coating is not 10 000 anymore but 50.

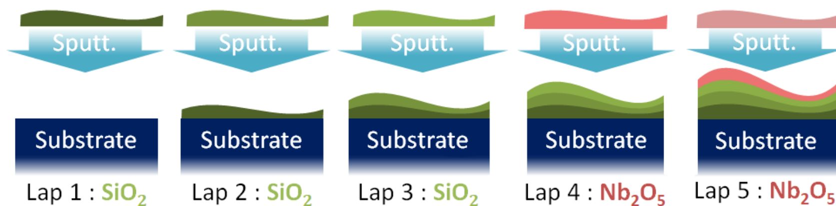

Figure 5: Illustration of the homothetic approach. In this example the non-uniformity profile for both sputters is equivalent. Relatively to the layer thickness, all the layers have the same non-uniformity profile.

In the framework of the *Euclid* project, L. Carminati (Airbus Defense and Space) has developed in 2016 a mathematical model based on the homothetic assumption. As the relative TFEs are all equal, we can consider each point of the coating as the nominal stack with a constant scale factor. Applying a thickness scale factor "α" to a coating leads to a spectral deviation of this coating's optical response (at first approximation) including then a phase shift. To sum up, each point (x, y) of the surface undergoes a scale factor $\alpha(x, y)$ applied to each layer, leading to a phase shift in reflection:

Downloaded From: https://www.spiedigitallibrary.org/conference-proceedings-of-spie on 06 May 2023
Terms of Use: https://www.spiedigitallibrary.org/terms-of-use

$$\varphi_{\mathrm{R}}'(x,y,\lambda) = \varphi_{\mathrm{R}}[\lambda * \alpha(x,y)^{-1}]\,. \tag{3}$$

This property is a key point to establish a direct linear relation between the WFE and the TFE. From that, Carminati has succeeded expressing this link with a chromatic function:

$$\mathrm{WFE}(x,y,\lambda) = K(\lambda)\,\mathrm{TFE}(x,y)\,, \tag{4}$$

with "K" a function that can be expressed from the known nominal total thickness and nominal phase shift. From that, a measure of the WFE at one wavelength only is enough to retrieve the TFE and thus fit the whole coating model.

The existing literature allows us to easily express the chromatic component of the WFE as a function of the TFE, thanks to this very simplified consideration. The first part of our own work was to use this relation to check whether a fit of the WFE is possible with the Fig.4 pipeline. We have numerically created "fake" WFE measurements (before having the bench at our disposal) and tried to apply the fit by reconstructing the corresponding TFE. The "fake" WFE is, in this case, generated by a stack which TFEs are expressed with random Zernike polynomials, but homothetic. The objective was only to see if in this simplified case, the fit was efficient. The fit Figure of Merit (FOM) is expressed as the maximum spatial standard deviation (in nm RMS) between the "fake" measured WFE: $\mathrm{WFE}_{\mathrm{mes}}(x,y,\lambda)$ and the modelled WFE: $\mathrm{WFE}_{\mathrm{mod}}(x,y,\lambda)$ along the whole spectral range. In our case, the FOM is below 0.1 nm RMS approximatively. The error on the WFE fit is thus very small compared for instance to the limit of 2 nm RMS of WFE knowledge allocated by ESA. All the steps of the fit pipeline are not detailed here and will be explained in the next part. However, we can conclude that the strategy is functional.

3.3 Double non-uniformity profile assumption

The homothetic hypothesis, described in the literature, is very accurate from a mathematical point of view and allows the simplification of the WFE/TFE relation, but has the major weakness of not being realistic enough. Indeed, it considers that uniformities in the layers made from the two materials are exactly the same. As the deposition of the materials is ensured by two different sputters with two different plumes, there is no reason to consider the Nb_2O_5 and SiO_2 non-uniformity profiles as equal. We therefore propose to use the same strategy but considering not one TFE for the whole stack but one TFE per material. In this more realistic case, the interaction between the WFE and the TFE is much more complicated. The previous mathematical approach is thus not applicable, as each point of the coating cannot be considered anymore as the nominal stack with a scale factor applied.

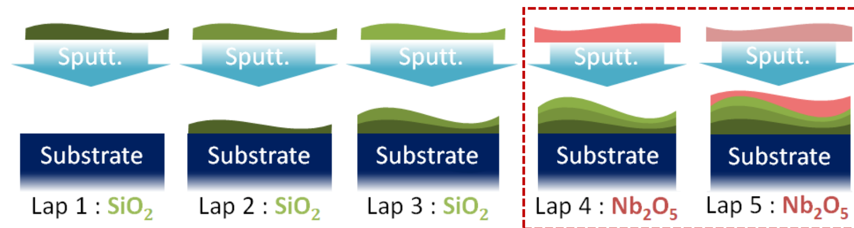

Figure 6: Illustration of the double-TFE profile (material-dependent) assumption. The non-uniformity profile is different for each sputter. The global structure is more complex to define than for a homothetic coating.

The major part of our work consists in implementing this new and more realistic hypothesis in our existing numerical model. Nevertheless, taking this hypothesis into account needs to use the coating characteristic matrix[11] "M" expression, on which depends the coating optical properties, especially φ_{R}. The matrix $M(\lambda,\gamma,Pol.)$ is the product of the characteristic matrix of each layer "j" (thickness d_j, index n_j) among N:

$$M(\lambda,\gamma,Pol.) \coloneqq \prod_{j=N}^{1} \begin{bmatrix} \cos(\delta_j) & i q_j^{-1} \sin(\delta_j) \\ i q_j \sin(\delta_j) & \cos(\delta_j) \end{bmatrix} \equiv \prod_{j=N}^{1} M_j(\lambda,\gamma_j,Pol.,n_j,d_j)\,, \tag{5}$$

where δ_j is the phase shift through the layer:

$$\delta_j(\lambda,\gamma_j,d_j,n_j) \coloneqq \frac{2\pi}{\lambda}\, n_j\, d_j \cos(\gamma_j)\,,$$

with γ_j is the refraction angle, expressed with the Snell-Descartes Relation:

$$n_j \sin(\gamma_j) = n_{\mathrm{air}} \sin(\gamma)\,,$$

Downloaded From: https://www.spiedigitallibrary.org/conference-proceedings-of-spie on 06 May 2023
Terms of Use: https://www.spiedigitallibrary.org/terms-of-use

and finally q_j is the admittance:

$$q_j(\lambda, \gamma_j, Pol.) \coloneqq \begin{cases} n_j \cos(\gamma_j), \text{s} - \text{polarization} \\ n_j \cos(\gamma_j)^{-1}, p - \text{polarization} \end{cases}.$$

In Eq. (5), each layer characteristic matrix $M_j(\lambda, \gamma_j, Pol., n_j, d_j)$, represents the link between the input and output electromagnetic field through the layer, and whose terms are related to the illumination properties (angle of refraction γ_j, wavelength λ, polarization $Pol.$). The characteristic matrix M represents thus the same link for the whole stack. In what follows, the polarization and angles of incidence as fixed, and then we consider only the spectral variation of $M(\lambda, \gamma, Pol.)$, denoted $M(\lambda)$.

Under homothetic assumption, there is thickness variation "$\alpha(x,y)\, d_j$" in all layers. With Eq. (3), it is possible to express linearly the dependence of the phase on this thickness variation without going through the matrix calculation in Eq. (5). In our case, there are two "combined" thickness variations depending on the layer material, and Eq. (3) is then not applicable.

After a deep analysis of the mathematical formalism underlying the thin-films physics, we succeeded in establishing the following linearization of the stack characteristic matrix M':

$$M'(x,y,\lambda) = M(\lambda) + A_{\mathrm{L}}(\lambda)\alpha(x,y) + A_{\mathrm{H}}(\lambda)\beta(x,y)\,. \tag{6}$$

In this expression, M and M' are the corresponding characteristic matrixes, for the nominal stack and the stack with non-uniformity respectively. The non-uniformities induced by each material (SiO_2 and Nb_2O_5) are now fully decoupled and described by their respective local scale factors $\alpha(x,y)$ and $\beta(x,y)$. The two known chromatic functions $A_{\mathrm{L}}(\lambda)$ and $A_{\mathrm{H}}(\lambda)$ can be expressed in function of the nominal stack properties and illumination properties (incidence, polarization, and wavelength), each function being linked to the Nb_2O_5 or SiO_2 properties. This relationship has been obtained especially with some Taylor-series decompositions, which remain valid if we consider two scale factors $\alpha, \beta \approx 1$ and no chromatic dependence of refractive indices. From the Eq. (6), it is possible to linearize the phase shift in reflection in the same way:

$$\varphi'_{\mathrm{R}}(x,y,\lambda) = \varphi_{\mathrm{R}}(\lambda) + \alpha(x,y)\, B_{\mathrm{L}}(\lambda) + \beta(x,y)\, B_{\mathrm{H}}(\lambda)\,. \tag{7}$$

This linearized expression gives the phase shift "with presence" of TFEs: $\varphi'_R(x,y,\lambda)$ in function of the same decoupled scale factors α, β and two known chromatic function $B_L(\lambda)$ and $B_H(\lambda)$. We now come back to an expression of the phase shift variation like in the Eq. (3) but extended to two variations. This expression was the last key to develop a "double TFE" dependence of the WFE, thus being:

$$\mathrm{WFE}(x,y,\lambda) = F_{\mathrm{L}}(\lambda)\, \mathrm{TFE_L}(x,y) + F_{\mathrm{H}}(\lambda)\, \mathrm{TFE_H}(x,y)\,. \tag{8}$$

The terms $\mathrm{TFE_L}(x,y)$ and $\mathrm{TFE_H}(x,y)$ are the non-uniformity profiles of SiO_2 and Nb_2O_5 respectively. Once again, the two chromatic functions $F_{\mathrm{L}}(\lambda)$ and $F_{\mathrm{H}}(\lambda)$ can be expressed with respect to the nominal stack properties and illumination conditions. The above expression is thus an equivalent of the "homothetic" $K(\lambda)$ transfer function (see Eq. 4), extended to two dependencies. Obviously, Eq. (6), (7), and (8) remain valid for the homothetic assumption. In that case, α is equal to β. We have chosen to not detail the full mathematical approach, as well as the analytical expression of the functions $F_{\mathrm{L}}(\lambda)$ and $F_{\mathrm{H}}(\lambda)$, which will deserve a dedicated publication. In this way, a "double TFE" profile fit is now possible. As the two TFEs are unknown, it needs logically at least two measured $\mathrm{WFE}(x,y,\lambda_i)$ to solve the following linear system:

$$\begin{bmatrix} \mathrm{TFE_L}(x,y) \\ \mathrm{TFE_H}(x,y) \end{bmatrix} = \begin{bmatrix} F_{\mathrm{L}}(\lambda_1) & F_{\mathrm{H}}(\lambda_1) \\ F_{\mathrm{L}}(\lambda_2) & F_{\mathrm{H}}(\lambda_2) \end{bmatrix}^{-1} \begin{bmatrix} \mathrm{WFE}(x,y,\lambda_1) \\ \mathrm{WFE}(x,y,\lambda_2) \end{bmatrix}. \tag{9}$$

This linear system allows us to retrieve each TFE and then fit the full coating model. Before continuing, it seems important to mention some aspects to this mathematical process.

Downloaded From: https://www.spiedigitallibrary.org/conference-proceedings-of-spie on 06 May 2023
Terms of Use: https://www.spiedigitallibrary.org/terms-of-use

3.4 Some details on the model mathematical approach

Above all, the choice of the two relevant wavelengths λ_1 and λ_2 is primordial. First, there are some obvious conditions related to system matrix inversion. In addition, the aforementioned system results from a linearization of the phase shift expression according to the two spatial deviations. Therefore a linearization error remains because this operation is itself performed after some mathematical simplifications, i.e. nulling nonlinear terms in Taylor-series decomposition. It is possible to determine for which wavelengths the linearization induces the fewest errors. The determination of λ_1 and λ_2 is a complex and essential step of the process, because the whole final performance of the fit depends on it. Such determination is also needed for the "homothetic" expression: Eq. (4), (with only one λ_{optim}), also obtained from mathematical simplifications. It is worth mentioning that the search for the best wavelengths to handle the linearization errors is tricky. Similar concerns have been encountered for the wavefront reconstruction at arbitrary wavelength developed by Venancio[22].

The other point we would like to highlight is the lack of information provided by the measurement itself. In practice, the WFE is evaluated by an integration of local slopes. Thus, the information about its own (non-zero) spatial mean value is ignored. For example, applying the fit under homothetic condition (see Eq. 4) results to some TFEs that also have zero average value. This is problematic because the "true" TFEs have a non-zero mean value. The stack is thus poorly reconstructed, and the resulting FOM will be poor, (more than 1 nm RMS). The solution to this problem is to implement a one-variable optimization. In brief, this optimization consists in "adding" this missing offset such as $T_{\text{mean}}/T_{\text{nom}}$, equal to "$a$", with T_{mean} the stack total average thickness, and T_{nom} the nominal thickness value. The resulting function $\text{FOM}(a)$ is thus minimized to 0.1 nm RMS approximatively (result presented previously in section 3.2). For the case of a fit with a TFE for each material, the same problem arises using Eq. (8). As there are two TFEs, there are 2 unknown offsets. In the same way, we implement a two-variable optimization to minimize the function $\text{FOM}(a_{\text{L}}, a_{\text{H}})$, with a_{L} and a_{H} being the two offsets.

3.5 Expected performance of the model under "double non-uniformity profiles" assumption

By using the previously detailed linear system (see Eq. 9), coupled to a bi-variable optimization, we expect to re-build the full coating with the right TFEs and the corresponding induced WFE. We tested three specific cases to generate a "sample" WFE, to be fitted by the two models.

- **First situation**: WFE from a stack considered homothetic. The chosen TFE is deduced from the non-uniformity maps measured by Optical Balzers Jena[9].

- **Second situation**: WFE from an "almost homothetic" stack. A Gaussian noise variation of 10% RMS now distinguishes the first 55 Zernike coefficients of the respective two TFEs. The Surface Figure Error (SFE) relative Peak-to-Valley (PTV) value is kept as 0.5%.

- **Third situation**: WFE from a stack with two totally distinct TFEs, whose respective 55 first Zernike coefficients are chosen randomly. The SFE relative PTV value is also kept as 0.5%.

For the first case there is only one run performed because of the absence of random variations. The obtained FOM is 0.08 nm RMS for homothetic fit and 0.02 nm RMS for "double TFE" fit. We can wonder why the double TFE fit is more efficient than the homothetic TFE fit if the reference stack is itself with homothetic TFEs. In both cases the TFE of the layers is fit with an extremely low relative residue, less than 0.05% RMS. This is the same for the residual of WFE. There is no real sense in comparing WFE residuals lower than 0.1 nm RMS. In this case the fit can be considered as "perfect", and the tiny residuals result from the numerical approximations that have been used in both pipelines.

Downloaded From: https://www.spiedigitallibrary.org/conference-proceedings-of-spie on 06 May 2023
Terms of Use: https://www.spiedigitallibrary.org/terms-of-use

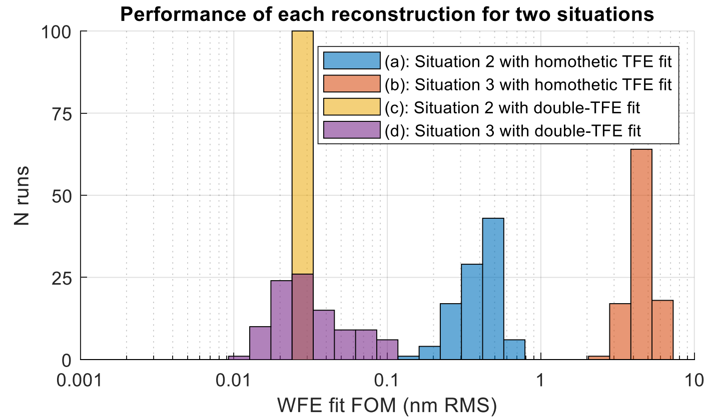

Figure 7: 4*100 *Runs performanc*e evaluation of “homothetic TFE” (a, b) and “double-TFE” (c, d) reconstructions applied to situations 2 and 3. For each run of situation 2, the reference TFEs are random modulations (10% RMS) of 55 first Zernike coefficients of situation 1’s TFE. For each run of situation 3, both TFE are randomly constructed with Zernikes, while respecting a relative PTV of 0.5%, representative of the dichroic manufacturing process.

By applying each fit to second and third cases (Fig. 7, 100 runs each), we can clearly see that the double TFE fit is always much more efficient. In the situation of a quasi-homothetic reference coating, the homothetic fit gives a still acceptable FOM (a) but is not as efficient as the double TFE fit (c). For the case of a double TFE reference stack, this difference in performance is even clearer, where the fit by homothetic approach is totally inefficient. Even the “best” FOM value is more than 1 nm RMS, (d).

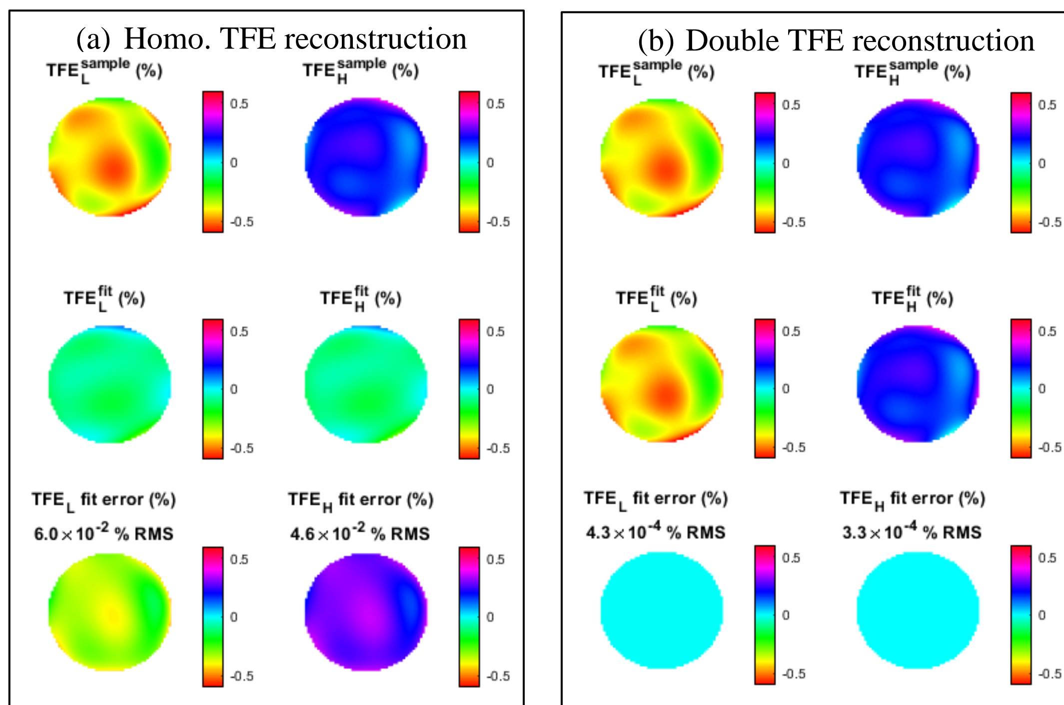

Figure 8 (left) example of Fig.7-(b) run. Figure 8 (right): example of Fig.7-(d) run. Each panel shows the relative TFE for each material (L, H) of the “sample” and the reconstructed coating. The fit residuals are also showed at the bottom.

Downloaded From: https://www.spiedigitallibrary.org/conference-proceedings-of-spie on 06 May 2023
Terms of Use: https://www.spiedigitallibrary.org/terms-of-use

The Fig. 8 provides a visual evidence of the two reconstructions effectiveness for a same "sample" coating. In both presented cases, the sample coating is created with uncorrelated TFEs (see the first line of each panel), generated with random Zernike polynomials. On the left panel, the homothetic fit is applied on the sample coating's induced WFE. The reconstruction is very poor, with $\mathrm{TFE}_{\mathrm{L}}^{\mathrm{fit}}$ and $\mathrm{TFE}_{\mathrm{H}}^{\mathrm{fit}}$ being now necessarily equal. The residuals maps (third line) show indeed the high difference between reference and fitted coating. For the WFE reconstruction, the resulting FOM is 3.55 nm RMS, in accordance with Fig. 7-(b) results. On the right panel, the double-TFE fit is used. This time, the reconstruction is way better, with some very low residuals. The resulting WFE's FOM is below 0.03 nm RMS. These results correspond to those presented in Fig. 7-(d).

3.6 Upcoming work on double-TFE model

The current work focuses on the model sensitivity to random errors. TFEs are systematic errors (even if they are defined randomly in the simulation) because they are identical for all layers (of the same material). The only difference is their PTV, weighted by their own thickness. On the other hand, purely random errors would be decorrelated from one layer to another. Such errors arise from an inaccuracy in the average thickness control during the coating manufacturing. Neither of the two proposed models take them into account. Since the nominal coating stack is considered in the analysis, the impact of deviations from the design must be assessed carefully.

Moreover, a deeper work will be to add some uncertainties to the fake "measured" WFE corresponding to the bench performance and to evaluate the consequences on the fit. Obviously, as soon as the bench is operational, we will use directly the actual WFE measured on the dichroic and evaluate the FOM of the fit for both models.

4. CONCLUSION

As presented in this document, a test bench and numerical reconstruction pipeline are being developed for the characterization of the WFE of the dichroic. Imagine Optic is developing the OBSERVE bench, fully compliant to the stringent tolerances and which will allow, from early 2023, the measurement of the reflected WFE at all wavelengths, incidence and polarizations with an accuracy below 2 nm RMS. In the meantime, we are developing at LMA a numerical model based on realistic assumptions and which will enable to compute the dichroic optical properties. Until now, first simulation results achieved a WFE reconstruction with an accuracy better than 0.1 nm RMS. Some other deeper performance analyses are planned in the upcoming months but these preliminary results are quite encouraging so far.

ACKNOWLEDGMENTS

The authors would like to thank IO team, developing the OBSERVE test bench under the ESA contract number: 4000135300/21/NL/PM. for their cooperation and expertise. This cutting-edge development managed by ESA for the *Euclid* mission implies stringent requirements to allow the characterization of complex coatings to an unprecedented scale to the author's knowledge.

The authors acknowledge the Euclid Consortium, the European Space Agency, and a number of agencies and institutes that have supported the development of *Euclid*, in particular the Academy of Finland, the Agenzia Spaziale Italiana, the Belgian Science Policy, the Canadian Euclid Consortium, the French Centre National d'Etudes Spatiales, the Deutsches Zentrum für Luft- und Raumfahrt, the Danish Space Research Institute, the Fundação para a Ciência e a Tecnologia, the Ministerio de Ciencia e Innovación, the National Aeronautics and Space Administration, the National Astronomical Observatory of Japan, the Netherlandse Onderzoekschool Voor Astronomie, the Norwegian Space Agency, the Romanian Space Agency, the State Secretariat for Education, Research and Innovation (SERI) at the Swiss Space Office (SSO), and the United Kingdom Space Agency. A complete and detailed list is available on the Euclid web site (http://www.euclid-ec.org).

Downloaded From: https://www.spiedigitallibrary.org/conference-proceedings-of-spie on 06 May 2023
Terms of Use: https://www.spiedigitallibrary.org/terms-of-use

REFERENCES

1 L. Amendola, S. Appleby, A. Avgoustidis et al. “Cosmology and fundamental physics with the *Euclid* satellite.” (Living Rev Relativ 21, 2 (2018). https://arxiv.org/abs/1606.00180 Euclid Definition Study Report ESA/SRE (2011)12: https://arxiv.org/abs/1110.3193

2 A. Refriegier, “Weak Gravitational Lensing by Large-Scale Structure”, (2003), Annual Reviews of Astronomy and Astrophysics 2003 – 41: 645–668, http://arxiv.org/abs/astro-ph/0307212v1

3 M. Kilbinger, “Cosmology with cosmic shear observations: a review”, (2015) Rep. Prog. Phys. 78 086901

4 R. Mandelbaum, “Weak Lensing for Precision Cosmology”, Annual Review of Astronomy and Astrophysics 56, nº 1 (2018): 393-433. https://doi.org/10.1146/annurev-astro-081817-051928.

5 Euclid Definition Study Report ESA/SRE (2011)12: https://arxiv.org/abs/1110.3193

6 Courtesy ADS, https://www.euclid-ec.org/?page_id=2639

7 M. Born, E. Wolf, “Principles of Optics”, 6th ed. Cambridge University Press, 1980

8 L. Venancio, L. Carminati, J. L. Alvarez, J. Amiaux, L. Bonino, J.-C. Salvignol, R. Vavrek, R. Laureijs, A. Short, T. Boenke, P. Strada, “Coating induced phase shift and impact on Euclid imaging performance”, (2016), Proc. of SPIE Vol. 9904

9 M. Lappschies, T. Weber, L. Venancio, S. Jakobs, “Advanced dielectric coatings for the *Euclid* mission telescope manufactured by the PARMS process”, Optical Interference Coatings (2016)

10 A. Thelen, “Design of optical interference coatings”, 1st ed. (McGraw-Hill, 1989), Chapter 2: Theory

11 Sh. A. Furnam, A.V. Tickhonravov, “Basics of optics of multilayer” 1st ed. (Editions Frontières, 1992), Chapter 1: Spectral characteristics of multilayer coatings: Theory

12 H. A. MacLeod, “Thin-Film Optical Filters”, 4th ed. (CRC press, 2010)

13 T. Weber, M. Lappschies, S. Jakobs, “Manufacturing of high performance VIS-NIR beam splitters by plasma assisted thin film deposition technologies”, Proc. SPIE 10691, Advances in Optical Thin Films VI, 106911A (2018); doi: 10.1117/12.2313459

14 M. Scherer, H. Hagedorn, W. Lehnert, J. Pistner, “Innovative production of thin film laser components” Proc. SPIE 5963, Advances in Optical Thin Films II, 596319 (2005); doi: 10.1117/12.625226

15 J. R. Fineup, “Phase Retrieval Algorithms: A Comparison”. Applied Optics 21, nº 15 (1982): 2758-69. https://doi.org/10.1364/AO.21.002758.

16 ISO-class for clean rooms: https://shieldscientific.fr/education-gants/2489/cleanroom-classifications/

17 LMA website: http://lma.in2p3.fr/

18 IO website: https://www.imagine-optic.com/imagine-us/

19 P. de Groot, “Measurement of transparent plates with wavelength-tuned phase-shifting interferometry” Appl. Opt. 39, 2658-2663 (2000)

20 P. Giacomo, “Propriétés chromatiques des couches réfléchissantes multi-diélectriques.” J. Phys. Radium, (1958), 19 (3), pp.307-311. 10.1051/jphysrad: 01958001903030700. jpa-00235839

21 A. V. Tikhonravov, M. K. Trubetskov, T. V. Amotchkina, “Investigation of the Error Self-Compensation Effect Associated with Broadband Optical Monitoring”. Applied Optics 50, nº 9 (2011): 113. https://doi.org/10.1364/AO.50.00C111.

22 L.M Gaspar Venancio, (European Space Agency), 2020, “Wave front reconstruction for dielectric coatings at arbitrary wavelength” (patent: US 2020/0348228 A1). UPSTO, https://pubchem.ncbi.nlm.nih.gov/patent/US-2020348228-A1

Downloaded From: https://www.spiedigitallibrary.org/conference-proceedings-of-spie on 06 May 2023
Terms of Use: https://www.spiedigitallibrary.org/terms-of-use